Title
Evaluating the calculated dry deposition velocities of reactive nitrogen oxides and ozone from two community models over a temperate deciduous forest

Journal
Atmospheric Environment, 45(16)

ISSN
1352-2310

Authors
Wu, Zhiyong
Wang, Xuemei
Chen, Fei
et al.

Publication Date
2011-05-01

DOI
10.1016/j.atmosenv.2011.02.063

Atmospheric Environment 45 (2011) 2663–2674

Contents lists available at ScienceDirect

Atmospheric Environment

journal homepage: www.elsevier.com/locate/atmosenv

Evaluating the calculated dry deposition velocities of reactive nitrogen oxides and ozone from two community models over a temperate deciduous forest

Zhiyong Wu [a,b], Xuemei Wang [a,*], Fei Chen [c], Andrew A. Turnipseed [c], Alex B. Guenther [c], Dev Niyogi [d], Umarporn Charusombat [d], Beicheng Xia [a], J. William Munger [e], Kiran Alapaty [f]

[a] School of Environmental Science and Engineering, Sun Yat-sen University, Guangzhou 510275, China
[b] Guangdong Provincial Key Laboratory of Environmental Pollution Control and Remediation Technology, Guangzhou 510275, China
[c] National Center for Atmospheric Research, Boulder, CO 80307, USA
[d] Purdue University, West Lafayette, IN 47907, USA
[e] School of Engineering and Applied Sciences and Department of Earth and Planetary Sciences, Harvard University, Cambridge, MA 02138, USA
[f] Atmospheric Modeling and Analysis Division, US Environmental Protection Agency, Research Triangle Park, NC 27711, USA

ARTICLE INFO

Article history:
Received 17 July 2010
Received in revised form
23 February 2011
Accepted 25 February 2011

Keywords:
Reactive nitrogen oxides
Ozone
Dry deposition velocity
WRF-Chem dry deposition module
Noah-GEM
1-D model

ABSTRACT

Hourly measurements of O_3, NO, NO_2, PAN, HNO_3 and NO_y concentrations, and eddy-covariance fluxes of O_3 and NO_y over a temperate deciduous forest from June to November, 2000 were used to evaluate the dry deposition velocities (V_d) estimated by the WRF-Chem dry deposition module (WDDM), which adopted Wesely (1989) scheme for surface resistance (R_c), and the Noah land surface model coupled with a photosynthesis-based Gas-exchange Evapotranspiration Model (Noah-GEM). Noah-GEM produced better $V_d(O_3)$ variations due to its more realistically simulated stomatal resistance (R_s) than WDDM. $V_d(O_3)$ is very sensitive to the minimum canopy stomatal resistance (R_i) which is specified for each seasonal category assigned in WDDM. Treating Sep-Oct as autumn in WDDM for this deciduous forest site caused a large underprediction of $V_d(O_3)$ due to the leafless assumption in 'autumn' seasonal category for which an infinite R_i was assigned. Reducing R_i to a value of 70 s m^{-1}, the same as the default value for the summer season category, the modeled and measured $V_d(O_3)$ agreed reasonably well. HNO_3 was found to dominate the NO_y flux during the measurement period; thus the modeled $V_d(NO_y)$ was mainly controlled by the aerodynamic and quasi-laminar sublayer resistances (R_a and R_b), both being sensitive to the surface roughness length (z_0). Using an appropriate value for z_0 (10% of canopy height), WDDM and Noah-GEM agreed well with the observed daytime $V_d(NO_y)$. The differences in $V_d(HNO_3)$ between WDDM and Noah-GEM were small due to the small differences in the calculated R_a and R_b between the two models; however, the differences in R_c of NO_2 and PAN between the two models reached a factor of 1.1–1.5, which in turn caused a factor of 1.1–1.3 differences for V_d. Combining the measured concentrations and modeled V_d, NO_x, PAN and HNO_3 accounted for 19%, 4%, and 70% of the measured NO_y fluxes, respectively.

1. Introduction

Global atmospheric emissions of nitrogen oxide have increased dramatically during the past 150 years, and the supply of reactive nitrogen to ecosystems has doubled due to anthropogenic activities such as nitrogen fertilization, biomass burning, and fossil fuel combustion (Galloway et al., 2008). Dry deposition is responsible for a significant portion of the total (wet and dry) nitrogen deposition (e.g. 34%, Munger et al., 1998; 58%, Sparks et al., 2008). Up to 43% of NO_x–N emissions over North America have been estimated to be removed from the atmosphere by dry deposition (Shannon and Sisterson, 1992). Reactive nitrogen oxides, called NO_y, is a class of oxidized nitrogen compounds including NO, NO_2, NO_3, N_2O_5, HNO_3, PAN (peroxyacetyl nitrate), other organic nitrates, and particle nitrate, which supply significant nutrient and acidic quantities to ecosystems. Augmented atmospheric deposition of NO_y associated with increased emissions of NO_x poses many environmental threats, including acidification of soil and surface water, eutrophication of lake, river and estuary, loss of biodiversity, damage to forests, and global climate change (Galloway et al., 2008). Increased anthropogenic emissions of NO_x combined with hydrocarbons have produced high levels of surface O_3 concentration. O_3 can penetrate the tissues

* Corresponding author. Tel.: +86 2084112293; fax: +86 2084113616.
E-mail address: eeswxm@mail.sysu.edu.cn (X. Wang).

1352-2310/$ – see front matter © 2011 Elsevier Ltd. All rights reserved.
doi:10.1016/j.atmosenv.2011.02.063

of leaves easily through stomatal uptake, causing stomatal occlusion and leaf damage. The direct uptake by vegetation through the stomata is also a major sink of O_3 in the lower troposphere (Turnipseed et al., 2009).

Given the significant impacts of NO_y and O_3 deposition on atmospheric chemistry and ecosystem health, it is desirable to quantify the deposition amount and assess the effects. Measuring deposition fluxes for reactive nitrogen compounds and O_3 with the eddy-covariance technique (e.g. Munger et al., 1996; Turnipseed et al., 2006) or the gradient method (e.g. Meyers et al., 1989; Sievering et al., 2001) have formed the basis for deposition models aimed at predicting dry depositions of reactive nitrogen compounds and O_3.

Models have been developed (e.g. Wesely, 1989; Meyers et al., 1998; Zhang et al., 2002, 2003; Niyogi et al., 2009; Wu et al., 2003) to estimate the dry deposition velocity (V_d) by commonly utilizing the resistance approach analogous to Ohm's law in electrical circuits. Accurately parameterizing the complex surface-atmosphere exchange process remains challenging for V_d modeling due to large variability in surface conditions (e.g., vegetation types, and soil contents) at model sub-grid scales. It is difficult to fully describe the physiological processes concerning the vegetation stomatal responses to various environmental conditions, leaf age, injury, and so on. The rapid within-canopy chemical reactions are not often considered in simple single-layer models, neither for the role of horizontal flow to receptor surfaces over non-uniform surfaces and terrains (Wesely and Hicks, 2000). Therefore, large uncertainties still exist in modeling V_d. A recent study (Flechard et al., 2010) modeled the V_d of inorganic reactive nitrogen species (i.e. NH_3, NO_2, HNO_3, and HONO and aerosol NH_4^+ and NO_3^-) over 55 monitoring sites throughout Europe, using four existing dry deposition models. Their result revealed that differences between models can reach a factor 2–3 and are even greater than differences between monitoring sites. Hence, there is a continuous need to evaluate modeled V_d over different land-cover types and for different chemical compounds.

Observational deposition fluxes of SO_2 and O_3 are often used to evaluate models (Zhang et al., 2002; Wu et al., 2003). However, few studies have evaluated modeled V_d for nitrogen species primarily because accurate quantifications of dry deposition fluxes and speciation of the reactive nitrogen species are difficult and expensive to obtain (Horii et al., 2005). Munger et al. (1996) demonstrated that the dry deposition fluxes of NO_y can be measured reliably using the eddy-covariance technique and year-round observations have been conducted at the Harvard Forest Environmental Measurement Site (HFEMS) since 1990. In a campaign attempting to estimate NO_y concentration and deposition budget, concentrations of individual NO_y species (i.e. NO, NO_2, PAN and HNO_3) have been measured at HFEMS. The reactive nitrogen dataset along with the O_3 fluxes/concentrations available at HFEMS are used to evaluate two community dry deposition models here.

One model is the Weather Research and Forecasting-Chemistry model (WRF-Chem) dry deposition module (hereafter WDDM). WRF-Chem is a state-of-the-art, regional atmospheric chemistry model (Grell et al., 2005) and has been successfully applied for regional air quality studies (Wang et al., 2009). Due to lack of observational data, few studies have evaluated the ability of the WDDM for calculating nitrogen V_d, even though dry deposition is one of the most important sinks for pollutants. The other model is the Noah land surface model (LSM) (Chen and Dudhia, 2001) coupled with a photosynthesis-based Gas-exchange Evapotranspiration Model (Niyogi et al., 2009) (hereafter Noah-GEM). The Noah LSM has been used to provide surface heat fluxes as boundary conditions for WRF. It is of broad interest to develop capacities of computing V_d in Noah LSM (Charusombat et al., 2010). This evaluation effort is part of a broader effort to eventually integrate the balance of hydrosphere, biosphere, and atmosphere with environmental modeling such as atmospheric nitrogen input for the ecosystems in Noah. There are also plans to couple surface deposition and emission information more closely in Noah by linking with biogenic emission models such as MEGAN (Model of Emissions of Gases and Aerosols from Nature; Guenther et al., 2006). So one main purpose of this paper is to document current deficiencies in WDDM and raise the awareness of such problems. Also, because an investigation of nitrogen deposition calculation has not been done for these models, this study takes advantage of recently available nitrogen flux data to investigate nitrogen-deposition algorithms, which can serve well in the deposition models. The objectives are to: 1) assess the performances of WDDM and Noah-GEM in calculating $V_d(NO_y)$ and $V_d(O_3)$ over a temperate deciduous forest, 2) understand the sensitivity of modeled $V_d(NO_y)$ and $V_d(O_3)$ to the key variables/parameters, and 3) improve the models by comparing with the field observations.

We will first describe the measurements used in this study (Section 2) and the modeling framework and formulations of WDDM and Noah-GEM (Section 3). Next, the observation data and model results and discussions are presented in Section 4, which is followed by the conclusions in Section 5.

2. Field measurements used in this study

2.1. Site description

The HFEMS is located in a temperate 80–100 year-old mixed deciduous forest in central Massachusetts (42.54 N, 72.18 W; elevation, 340 m), which consists of red oak (*Quercus rubra*), red maple (*Acer rubrum*) with scattered hemlock (*Tsuga canadensis*), red pine (*Pinus resinosa*), and white pine (*Pinus strobus*). The canopy height near the observation tower is approximately 20 m with a peak leaf area index (*LAI*) of 3.4 $m^2\ m^{-2}$ during summer. The nearest sources of significant pollution are a secondary road about 2 km west of the site and a main highway about 5 km north of it.

A permanent 30-m Rohn 25 G tower has been used at HFEMS to measure eddy-covariance fluxes of CO_2, NO_y, and O_3, along with vertical profiles of NO, NO_2, and O_3 since 1990. Measurements of PAN concentrations were added to the tower in 2000. A temporary 23-m steel scaffolding tower, situated about 100 m to the southeast of the Rohn tower, was configured with a Tunable Diode Laser Absorption Spectrometer (TDLAS) to measure concentrations of HNO_3 from June–November 2000. Due to physical constraints, the second tower did not match the measurement height of HNO_3 (22 m) with the measurement height of O_3, NO_y, NO, NO_2, and PAN (29 m) on the first tower. However, Horii et al. (2005) confirmed that the two datasets are spatially coherent on the hourly timescale. Details on the site and the instrumental methods can be found in Munger et al. (1996) and Horii et al. (2005). Data used in this study are available online at http://atmos.seas.harvard.edu/lab/data/nigec-data.html.

2.2. Calculations of flux and dry deposition velocity

The fluxes (F) of O_3 and NO_y were measured using the eddy-covariance technique. The ratio of observed heat flux and heat flux mathematically smoothed to simulate the attenuation of high-frequency variations by the instruments was used to account for loss of scalar covariances at high frequencies. Corrections were typically less than 20% (Munger et al., 1996; Horii et al., 2005). Flux data were also omitted during periods

of very low turbulence intensity (when the friction velocity, $u_* < 0.2\ \mathrm{m\,s^{-1}}$), resulting in approximately 18% and 21% of the data being omitted for O_3 and NO_y, respectively. In addition, periods with $[O_3] < [NO_y]$ (1%) were excluded for O_3 to avoid periods when O_3 chemical reactions may exceed O_3 deposition (Munger et al., 1996).

Assuming a zero concentration on the absorbing surface, the dry deposition velocity (V_d) can be determined as

$$V_d(z) = -F/C(z) \quad (1)$$

where $C(z)$ is the gas concentration at a reference height, z.

3. Description of models

3.1. Modeling framework

The resistance method determines V_d as the reciprocal of a total resistance (R_t) which consists of a series of resistances to perform gas transport from the atmosphere down to the surface.

$$V_d(z) = R_t^{-1} = (R_a(z) + R_b + R_c)^{-1} \quad (2)$$

Table A.1 describes each resistance component, and Table A.2 compares the formulations between WDDM and Noah-GEM.

3.2. Further developments of GEM

The GEM model (Niyogi et al., 2009) was further developed here (see Appendix B), but the parameters were kept the same and not specifically tuned for this study. R_s is the primary output of GEM and since direct measurements of R_s were not available at HFEMS, examining modeled surface heat fluxes provides an independent assessment of R_s. The new results from the Noah-GEM model with modified R_s substantially improved calculations of heat fluxes for both summer and autumn (Fig. 1), implying that it produced more reasonable R_s and better surface energy partitioning between sensible and latent heat fluxes. In section 4, we discuss the performance of Noah-GEM in calculating $V_d(O_3)$ and $V_d(NO_y)$, based on this modified version.

3.3. Model configuration

The WDDM was extracted from the WRF-Chem model V3.1.1 and executed in a 1-D mode, and the Noah LSM V3.1 plus GEM was executed in the same fashion. Hourly tower measurements of air temperature (T_a), relative humidity (RH), wind speed (WS), wind direction (WD), atmospheric pressure (P_a), downward shortwave radiation (R_{g_in}), downward long-wave radiation (R_{long_in}), and precipitation rate (P_{recip}) at the height of 29 m were used to drive Noah-GEM. The u_* and L are obtained in Noah via an iterative process, using T_a, RH, WS, and P_a (Chen et al., 1997). WDDM requires inputs of T_a, R_{g_in}, RH and P_{recip} from observations, and u_*, and L calculated by Noah. Hourly V_d were computed for O_3, NO, NO_2, PAN and HNO_3.

3.4. Modeling analysis

Model results are evaluated using descriptive statistics such as the degree of agreement (d) and fractional bias (FB) (e.g., Charusombat et al., 2010):

$$d = 1 - \sum_{i=1}^{n}(o_i - m_i)^2 \Big/ \sum_{i=1}^{n}(|o_i| + |m|_i)^2, \quad (3)$$

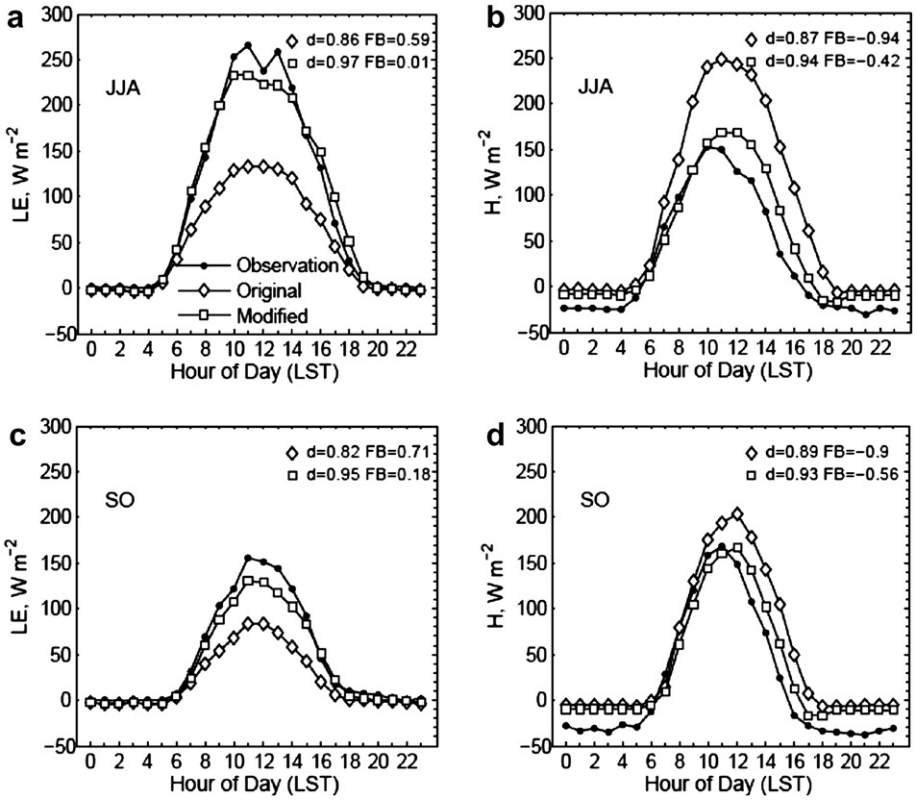

Fig. 1. Comparison of averaged diurnal cycles of observed and modeled heat fluxes by Noah-GEM. (a) Latent heat flux for June–August, (b) sensible heat flux for June-August, (c) latent heat flux for September-October, and (d) sensible heat flux for September–October. *d* and *FB* were calculated from the original hourly data.

$$\mathrm{FB} = 2\left(\sum_{i=1}^{n} o_i - \sum_{i=1}^{n} m_i\right) \Big/ \left(\sum_{i=1}^{n} o_i + \sum_{i=1}^{n} m_i\right), \quad (4)$$

where o_i is the observation, m_i the model result, and n the number of samples.

4. Results and discussion

4.1. The observations of O_3 deposition and its environmental drivers

Fig. 2 shows the time series of hourly-averaged [O_3] and $F(O_3)$ from June–October 2000. There was a distinct seasonal cycle of [O_3] showing maxima in summer, associated with the high solar radiation and temperature. The peak values ranged from 40 to 80 ppbv, slightly lower than the observations in 1991–1994 (Munger et al., 1996). $F(O_3)$ followed the same seasonal trend with maxima during summer, closely coinciding with high concentrations and canopy growth (Munger et al., 1996). As shown in Fig. 3, $V_d(O_3)$ augmented with increasing *PAR* (when $<1400\ \mu mol\ m^{-2}\ s^{-1}$) and decreased with increasing *VPD*. At moderate temperature (8–24 °C), $V_d(O_3)$ exhibited relatively small variations, but declined at more extreme temperature conditions. The environmental factors are often not independent from each other, e.g., high *PAR* often accompanying high temperature and *VPD*. $V_d(O_3)$ tended to decrease with increasing *PAR* above $1400\ \mu mol\ m^{-2}\ s^{-1}$, suggesting that temperature and *VPD*, rather than light, take controls in regulating stomatal openings. $V_d(O_3)$ increased almost linearly with increasing latent heat flux (*LE*), consistent with stomatal control of the O_3 uptake and plant evapotranspiration. These trends agree with the analysis by Turnipseed et al. (2009) over a subalpine forest. $V_d(O_3)$ had a strong diurnal cycle. During summer, mean $V_d(O_3)$ peaked before 1200 LST at $0.9\ cm\ s^{-1}$ and dropped throughout the day to minimum value of $0.2\ cm\ s^{-1}$ at night (Fig. 4), as seen in Munger et al. (1996).

4.2. Evaluation of modeled $V_d(O_3)$

Fig. 4 compares the modeled summer $V_d(O_3)$ by WDDM and Noah-GEM against observations. Table 1 presents the statistical results of the comparison. WDDM and Noah-GEM produced low values of $V_d(O_3)$ at night ($\sim 0.1\ cm\ s^{-1}$), much smaller than the observations (FB = 0.43–0.82). Zhang et al. (2002) and Charusombat et al. (2010) reported a similar bias, indicating an overestimation of nighttime non-stomatal resistance (R_{ns}). Wesely (1989) scheme estimates R_{ns} mainly using constant values specified for each season and each land-use category, while a recent R_{ns} scheme developed by Zhang et al. (2003) is a function of u_*, *RH*, *LAI* and canopy wetness for non-stomatal uptake. As the main purpose of this paper is to compare the performance of different algorithms for stomatal uptake, Noah-GEM deploys the same R_{ns} parameterization as WDDM for convenience of comparison. The performance of Noah-GEM and WDDM can be improved by utilizing the more realistic and accurate R_{ns} parameterization (e.g. Zhang et al., 2003) in the future work.

$V_d(O_3)$ increased in the morning as canopy photosynthesis became active. In Fig. 4, WDDM and Noah-GEM produced $V_d(O_3)$ with similar magnitude. However, WDDM did not capture the peak and underestimated morning $V_d(O_3)$ by $\sim 0.2\ cm\ s^{-1}$. Noah-GEM, on the other hand, was able to capture the $V_d(O_3)$ decline possibly as a result of stomatal closure at noon. Noah-GEM also produced a second peak in $V_d(O_3)$ in the late afternoon that was not observed. Zhang et al. (2006) also observed the early morning peak of $V_d(O_3)$ over two forest sites and proposed a threshold of accumulated O_3 stomatal flux for leafs, above which stomatal uptake of O_3 is slowed down probably due to an increased substomatal CO_2 concentration or non-zero O_3 concentrations inside the stomata. However, those factors are not considered in the current deposition models.

In Fig. 5, the observed $V_d(O_3)$ showed expected patterns of behavior with respect to the main environmental drivers (*PAR*, temperature and *VPD)* and, therefore, exhibited both unimodal (June 03, 16, and 18) and bimodal diurnal patterns (June 04, and 17). Noah-GEM captured the bimodal diurnal pattern on June 04 and 17, while under the unimodal conditions it reproduced the peak before noon but overestimated the afternoon O_3 uptake. WDDM was found to hardly capture the diurnal behaviors of $V_d(O_3)$, probably due to its Jarvis-type R_s (Eq. (A8)). However, it should be pointed out that Wesely (1989) R_c scheme was developed for general application, which requires very little data to use and intends to produce average estimate for a long time over large areas, rather than a period of days at a particular site.

WDDM considerably underestimated $V_d(O_3)$ in autumn (Fig. 6), and the minimum canopy stomatal resistance (R_i, which is also broadly denoted as R_{smin} in the atmospheric and plant modeling community) was found to be responsible for this large discrepancy. The R_i parameter in WDDM for deciduous broadleaf forests was assigned to be an infinite value ($10^{25}\ s\ m^{-1}$ was used) for early autumn (Wesely, 1989). Here we defined the season classification for June–August as category 1(summer) and September–October as seasonal 2 (early autumn) respectively, based on the general climate at HFEMS (see also Munger et al., 1998). The infinite R_i implies that there is no air-surface exchange via the stomatal pathway (Wesely, 1989) and is only valid for leafless condition. However, this was not the case for the Harvard Forest during September–October, as indicated by the observations of net ecosystem exchange of CO_2 and also *LAI* (Urbanski et al., 2007). The dominant effect of R_i on modeled R_s has been emphasized (e.g. Cooter and Schwede, 2000) and is well illustrated in Fig. 6. For this particular study, the value of R_i for summer ($70\ s\ m^{-1}$) seems appropriate for the early autumn.

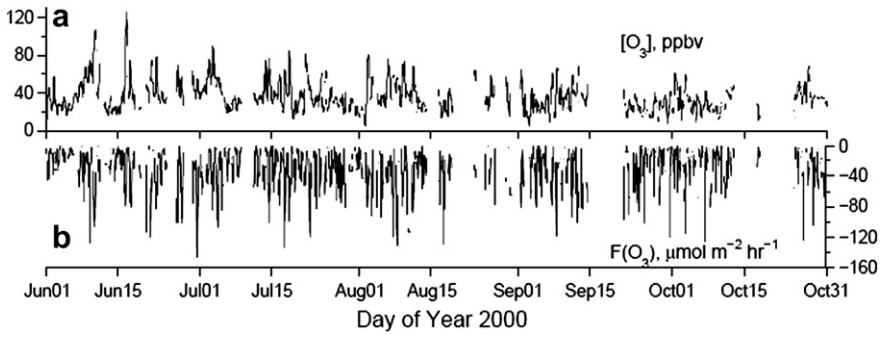

Fig. 2. Time series of (a) O_3 mixing ratio, and (b) O_3 fluxes.

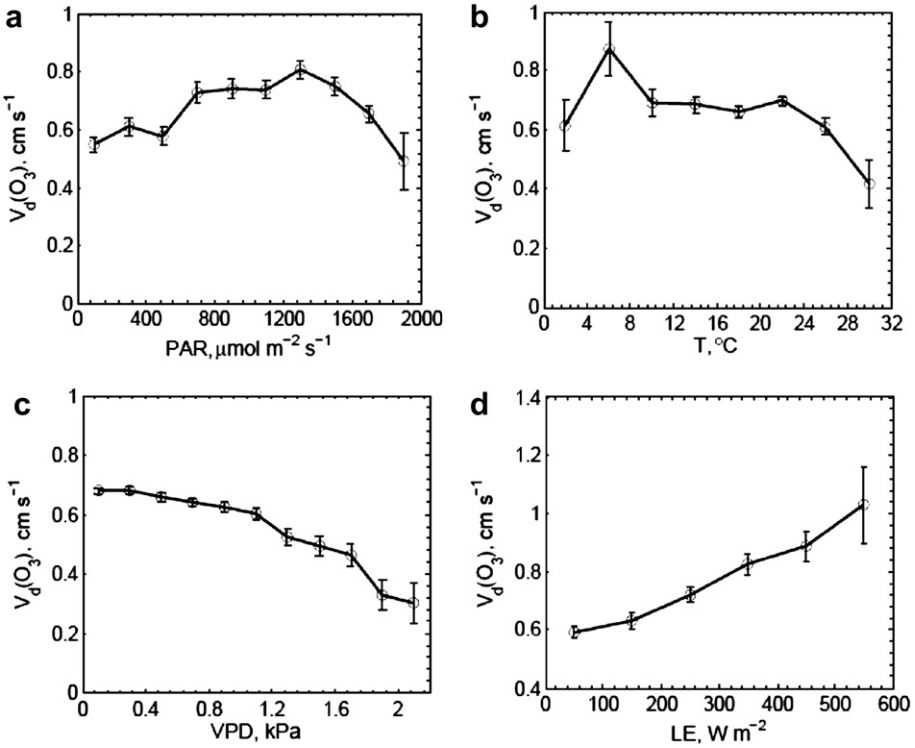

Fig. 3. Plots of mean daytime O_3 deposition velocity binned as a function of (a) photosynthetically active radiation, (b) air temperature, (c) vapor pressure deficit, and (d) latent heat flux. Error bars indicate standard error of the mean ($\sigma/N^{1/2}$). Daytime is 9:00–17:00 (LST).

Fig. 6 shows that neither model captured the rising of $V_d(O_3)$ in the early morning hours (0300–0600 LST). The early morning rising is possibly due to some factors (e.g. episodic mixing events and transport) which are not adequately represented by the resistance analogy, and also note that the small number of observations available during this period is likely hard to smooth those effects.

As illustrated by Fig. 6, the uncertainty in specifying R_i is one main reason for modeled bias in R_s and V_d of gases that are under stomatal control for WDDM. However, the prescription of R_i inherently has significant uncertainty because R_i cannot be measured or determined independently in the laboratory (Niyogi et al., 2009) and also the assumption of a constant R_i value within a season is inappropriate because of its temporal variations including diurnal cycle (Avissar, 1993). Better approaches have been proposed to solve the issue related with seasonal category classification, such as using continuous *LAI* without the need of defining different seasonal categories (e.g., Zhang et al., 2003), which could avoid the abrupt change of input parameters (e.g., R_i) from one season to the next. Charusombat et al. (2010) identified *LAI* as the first-order parameter affecting Noah-GEM estimates of R_s. The Noah LSM prescribed a maximum value of 3.3 m^2 m^{-2} for *LAI* in this case, slightly lower than the field measurement (3.4 m^2 m^{-2}). Model performance can be improved by assimilating more accurate and seasonally-varying *LAI* data in the future work.

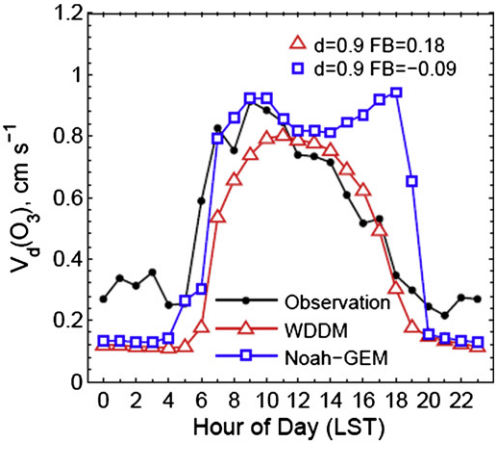

Fig. 4. Comparison of averaged diurnal cycles of observed and modeled O_3 deposition velocities by WDDM and Noah-GEM during June–August. *d* and *FB* were calculated from the original hourly data.

R_s is a complex and dynamic variable representing the coupled effects of resistance imposed by plants to vegetation-atmosphere exchange through leaf stomata (Niyogi et al., 2009). The difference between modeled $V_d(O_3)$ by WDDM and Noah-GEM is mainly caused by the use of different R_s schemes. Noah-GEM simulates the response of stomata to various environmental variables (e.g. *PAR*, canopy temperature, soil moisture, CO_2 concentration and relative humidity at the leaf surface) (Niyogi et al., 2009). A significant feature of Noah-GEM is that it is structured to consider the impacts of physiological

Table 1
Statistical results of the observed and modeled $V_d(O_3)$ and $V_d(NO_y)$.[a]

		All		Daytime		Nighttime	
		d	FB	*d*	FB	*d*	FB
$V_d(O_3)$	WDDM	0.90	0.18	0.93	0.01	0.62	0.82
	Noah-GEM	0.90	−0.09	0.93	−0.18	0.70	0.43
$V_d(NO_y)$	WDDM	0.86	0.48	0.92	0.16	0.61	1.09
	WDDM*	0.88	0.38	0.94	0.04	0.61	1.09
	Noah-GEM	0.88	0.37	0.94	0.02	0.58	1.18

[a] Note: Daytime is 0900–1700 (LST); Nighttime is 1900–0600 (LST). The sample numbers are 1134, 551 and 430 for $V_d(O_3)$, and 170, 80 and 70 for $V_d(NO_y)$, respectively.

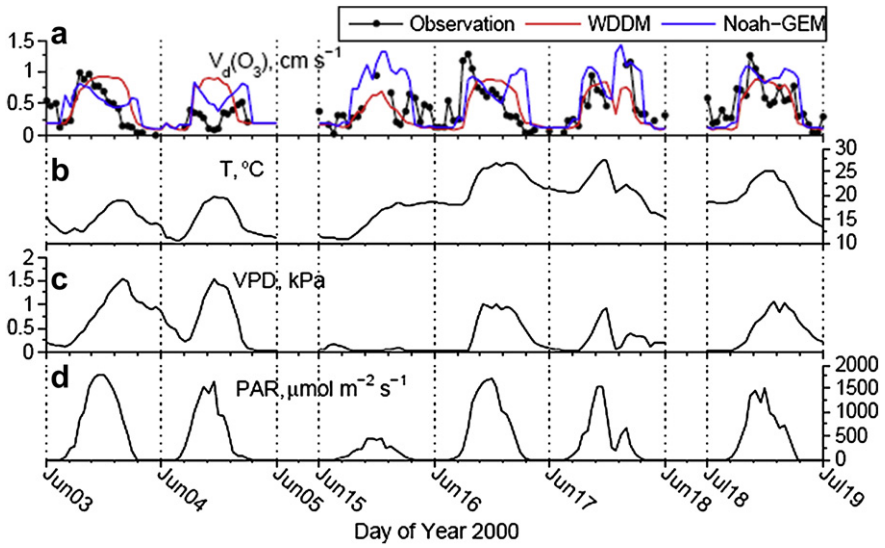

Fig. 5. Time series of (a) observed and modeled O_3 deposition velocities by WDDM and Noah-GEM, (b) air temperature, (c) vapor pressure deficit, and (d) photosynthetically active radiation.

processes including CO_2 assimilation rate on the responses of leaves to environmental parameters, which can predict R_s better than the Jarvis-style approach that is based on the minimum canopy stomatal resistance parameter (Niyogi et al., 2009).

4.3. The observations of NO_y deposition and its environmental drivers

HFEMS experienced minor pollution events during the selected period (Fig. 7). [NO_y] was generally lower than 5 ppbv, occasionally reaching 15 ppbv. $F(NO_y)$ and $V_d(NO_y)$ showed large day-to-day variations, with maximum values of 22 µmol m^{-2} h^{-1} and 4.5 cm s^{-1}, respectively. $F(NO_y)$ and $V_d(NO_y)$ tended to peak during midday, consistently following similar diurnal behavior to those of turbulence development. Large values of $V_d(NO_y)$ on October 02, 04, 07 and 08 accompany large ratios of HNO_3/NO_y, inferring a key role HNO_3 played in the NO_y deposition and $V_d(NO_y)$ (see also Munger et al., 1996).

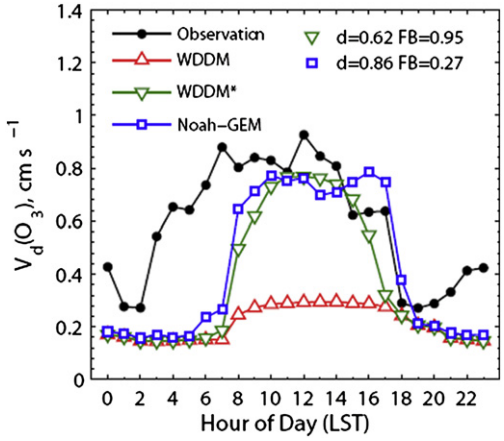

Fig. 6. As in Fig. 4, but for September–October. 'WDDM' indicates the simulation results with R_i of 10^{25} s m^{-1}, which was assigned to early autumn in WDDM. 'WDDM*' indicates the simulation results with R_i of 70 s m^{-1}, which was assigned to summer in WDDM.

The measured $V_d(NO_y)$ represent averaged V_d of the total NO_y species. But, in current gas dry deposition models, V_d values are estimated for individual species (see Section 3). Similar to Michou et al. (2005), the concentrations and V_d of individual NO_y species were used to derive a composite $V_d(NO_y)$, which can be more directly compared to observations. Simulated $V_d(NO_y)$ can be defined as

$$V_d(NO_y) = \sum_{i=1}^{n}[x_i]V_d(x_i) \Big/ \sum_{i=1}^{n}[x_i], \quad (5)$$

where x_i is the member of the NO_y family, and n the number of the members.

Modeling-wise, the unique value of this data set at HFEMS lies in the availability of the simultaneous concentrations of the main NO_y species (e.g., NO, NO_2, PAN, HNO_3) and the high temporal resolution (1 h). However, data gaps exist in the concentration measurements especially for HNO_3, which is very difficult to measure at a short integration time (e.g., at hourly interval) due partially to its tendency to adsorb onto surfaces (Horii et al., 2005). All the gaps in the concentrations will be reflected in the simulated $V_d(NO_y)$ (see Eq. (5)). To obtain a less patchy simulation of $V_d(NO_y)$, a "x/NO_y" ratio method was used to fill the gaps. The average diurnal cycles of "x/NO_y" were derived from the measurements from June–November 2000 (not shown here). Along with the NO_y concentrations, inferred concentrations of NO, NO_2, PAN, and HNO_3 were derived as

$$[x_i]^{D,H}_{\text{inferred}} = [NO_y]^{D,H} \times \text{Ratio}\left([x_i]/[NO_y]\right)^{H}, \quad (6)$$

where D indicates the date, H is the hour of day ($H = 0,1,2,\ldots,23$), $[NO_y]^{D,H}$ is the measured concentration of NO_y at the hour of H, on the date of D, $[x_i]_{\text{inferred}}$ is the inferred concentration of x_i, and Ratio $([x_i]/[NO_y])^H$ is the averaged ratio at the hour of H.

The inferred concentrations were used to fill the gaps in the measured concentrations. Observations at HFEMS suggested that HNO_3 played a critical role in $V_d(NO_y)$. To minimize the errors in simulated $V_d(NO_y)$ that result from inferred concentrations, the period (October 1–12, shown in Figs. 7 and 8) with the fewest gaps in HNO_3 concentrations was selected.

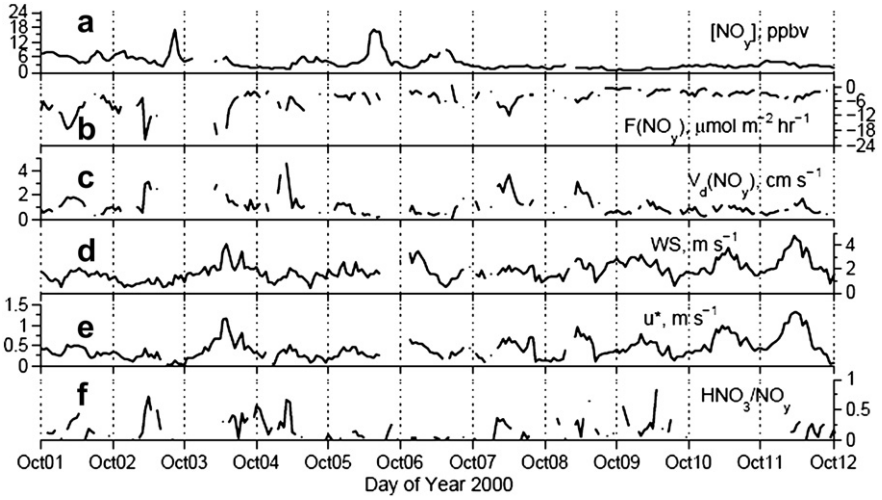

Fig. 7. Time series of (a) NO_y mixing ratio, (b) NO_y fluxes, (c) NO_y dry deposition velocities, (d) wind speed, (e) friction velocity, and (f) the ratio of HNO_3/NO_y.

Fig. 8 presents the measured concentrations of the NO_y species and also the gap-filled data from the "x/NO_y" ratio method. A few gaps existed for NO and NO_2 while PAN concentrations were all inferred. Given that PAN usually showed a relatively small V_d, and the averaged PAN/NO_y ratio had a relatively small deviation, the simulated $V_d(NO_y)$ should not be significantly affected by the uncertainties in the inferred PAN concentrations. The relative differences between the concentrations of NO_y and the sum of gap-filled NO, NO_2, PAN and HNO_3 were typically less than 30% (Fig. 8a).

4.4. Evaluation of modeled $V_d(NO_y)$

The roughness length for momentum (z_0) is an essential parameter in calculating R_a in LSMs and can be prescribed as a function of land-cover type, as in Noah where the value of 0.5 m is assigned for deciduous broadleaf forest. Alternatively, if information about the vegetation morphology (e.g., canopy height (h_c), and *LAI*) is known, z_0 can be calculated following Meyers et al. (1998):

$$z_0 = h_c\left(0.215 - \mathrm{LAI}^{0.25}/10\right), \tag{7}$$

or simply assumed 0.1 h_c (e.g., Chen and Zhang, 2009). In our sensitivity simulations, the model was run with three z_0 values: 1) 0.5 m (Noah default), 2) 1.6 m (Eq. (7)) and 3) 2 m (0.1 h_c). As z_0 increased from the initial model value of 0.5 to 1.6 and 2 m, modeled u_* increased significantly and approached observations (Fig. 9). Increased z_0 and u_* can reduce R_a and R_b (Eqs. (A3) and (A7)), which, in turn, leads to an increase of up to 1.5 cm s^{-1} in modeled $V_d(NO_y)$. This exercise demonstrates that adjusting z_0 can substantially alter the V_d of compounds sensitive to R_a and R_b (e.g. HNO_3). Ultimately, a value of 2 m for z_0 seems a reasonable representation of the canopy structure for HFEMS in this scenario. WDDM showed similar response to the parameter z_0, and the results are not presented here. Hereafter, we assessed the models performance with z_0 set to 2 m.

These sensitivity tests highlight the importance of treating the atmospheric surface layer in modeling the biosphere-atmosphere exchange. Indeed, current LSMs (including WDDM and Noah) employ the Monin–Obukhov Similarity Theory (MOST) to parameterize surface exchange coefficients. While MOST provides a dimensionally-based set of relationships that links the vertical fluxes of scalars to the gradients of the mean profiles within the

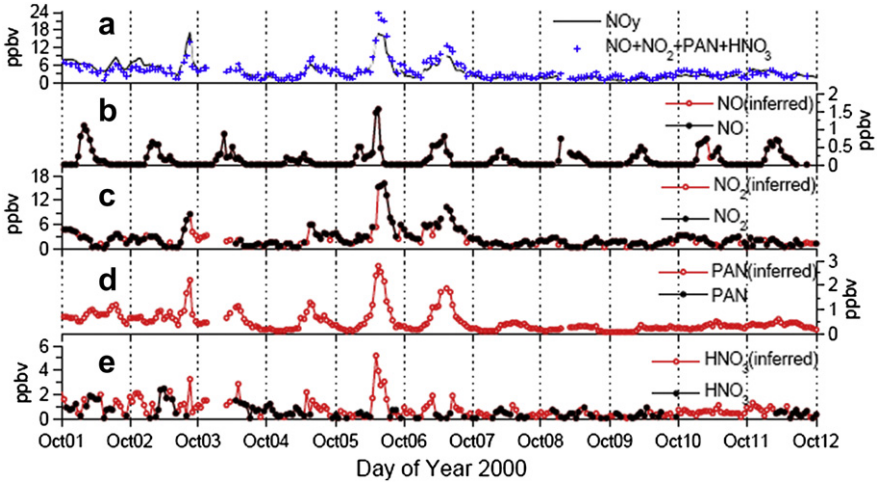

Fig. 8. Time series of the (a) NO_y mixing ratio and the sum of the mixing ratios of NO, NO_2, PAN, and HNO_3, (b) NO mixing ratio, (c) NO_2 mixing ratio, (d) PAN mixing ratio, and (e) HNO_3 mixing ratio. The black filled cycles are the measurements and red open circles are the inferred concentrations by the "x/NO_y" ratio method (For interpretation of the references to color in this figure legend, the reader is referred to the web version of this article.).

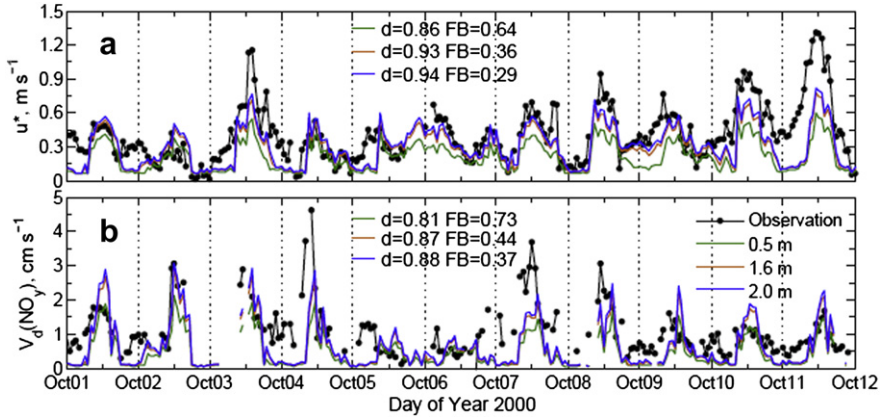

Fig. 9. Sensitivity of Noah-GEM modeled friction velocity and NO_y deposition velocity to z_0 parameter: observation (black line, cycle symbol); $z_0 = 0.5$ m (green line); $z_0 = 1.6$ m (yellow line); $z_0 = 2$ m (blue line) (For interpretation of the references to color in this figure legend, the reader is referred to the web version of this article.).

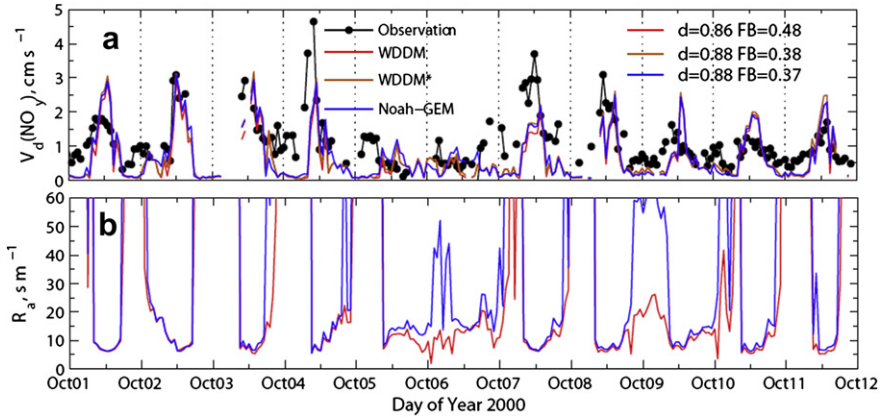

Fig. 10. (a) Comparison of a time series of observed and modeled NO_y deposition velocity by WDDM and Noah-GEM, and (b) modeled R_a by WDDM and Noah-GEM (using $z_0 = 2$ m).

atmospheric surface layer, it is only valid well above the rough surface (Högström, 1996) and fails in the so-called roughness sublayer, which is above tall canopies and within canopies (e.g., Harman and Finnigan, 2008). Simply adjusting parameters such as z_0 used in MOST may not solve this fundamental problem, and future work to improve the models will involve the use of vertically-varying profiles of mean scalar concentration (e.g., Harman and Finnigan, 2008) or a multi-layer canopy model that explicitly resolves the radiative, dynamical, and thermal transport within vegetation canopies.

Fig. 10a compares the modeled $V_d(NO_y)$ by WDDM and Noah-GEM against the observations. Table 1 presents the statistical results of the comparison. As described in section 4.2, WDDM prescribed an infinite value for R_i, which results in no air-surface exchange via stomata during autumn. To assess the sensitivity of R_s parameterization to $V_d(NO_y)$ estimate, we conducted an additional simulation, reducing R_i to 70 s m^{-1} as validated in $V_d(O_3)$ study. The WDDM modeled daytime $V_d(NO_y)$ increased from 1.2 cm s^{-1} to 1.37 cm s^{-1} (on average), closer to the observations of 1.41 cm s^{-1} (also see Table 1, *FB* decreased from 0.16 to 0.04). This result is consistent with Munger et al. (1996) in that the stomatal influence on NO_y dry deposition at HFEMS is relatively small. WDDM with corrected R_i presented quite similar results with Noah-GEM (Table 1 and Fig. 10), as WDDM has the same expressions for R_b, R_m, and R_{ns} with Noah-GEM and the predicted R_a values by the two models are generally close.

Although the models are generally in good agreements with the observations ($d = 0.88$), they seem to underestimate the nighttime value of $V_d(NO_y)$ significantly (FB = 1.09–1.18). Overestimation of nighttime R_a may be a chief reason for this unsatisfactory model performance as the conventional micrometeorological equations (e.g. Eqs. (A2), (A3)) have been known to have poor R_a estimate for nighttime stable regime (Wesely and Hicks, 2000). The underestimation of $V_d(HNO_3)$ in turn caused the poor performance of $V_d(NO_y)$ during nighttime. Part of these model deficiencies can also be attributed to the fact that both models do not have a multiple canopy scheme to represent a realistic wind shear within forest canopies.

Models reproduced the daytime $V_d(NO_y)$ with satisfactory statistic results ($d = 0.94$, FB = 0.02–0.04), and captured most variations in the observation (Fig. 10a), while the bias occurred

Table 2
Median of the modeled deposition velocity (surface resistance) in summer.

	Morning (0800–1000 LST)		Noon (1100–1300 LST)		Afternoon (1400–1600 LST)	
	NO_2	PAN	NO_2	PAN	NO_2	PAN
WDDM	0.65[a] (131[b])	0.43 (206)	0.69 (128)	0.45 (200)	0.60 (145)	0.40 (226)
Noah-GEM	0.86 (89)	0.58 (141)	0.64 (138)	0.42 (216)	0.70 (121)	0.47 (189)

[a] V_d, cm s^{-1}.
[b] R_c, s m^{-1}.

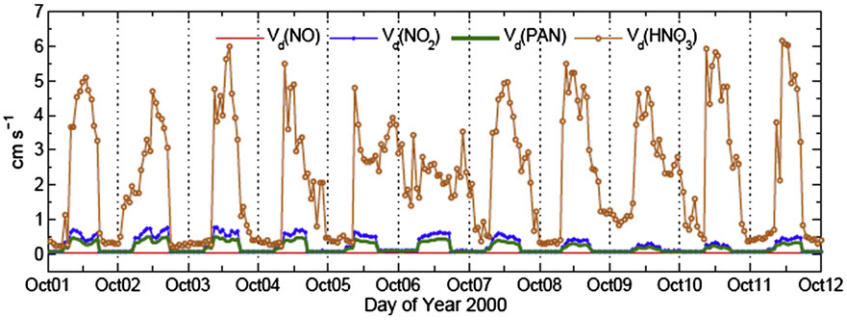

Fig. 11. Modeled deposition velocities for NO_y species by Noah-GEM (using $z_0 = 2$ m).

mainly on October 04, 07 and 08. The underestimation of u_* on October 07 and 08 (Fig. 9a) leaded to a too high R_a, which could be one reason for the $V_d(NO_y)$ underestimation. A large ratio of HNO_3/NO_y was observed (Fig. 7) on October 04, which caused the large $V_d(NO_y)$ in the observations. The models appear to substantially underestimate the HNO_3 deposition on this particular day.

At HFEMS, HNO_3 dominated the NO_y deposition, so the modeled $V_d(NO_y)$ did not show much sensitivity to R_s, but mostly depended on R_a and R_b. However, a recent field study over a coniferous forest (Turnipseed et al., 2006; Sparks et al., 2008) estimated that HNO_3 accounted for only ~24% of the NO_y flux and PAN exhibited a close portion of ~20%. Zhang et al. (2009) investigated the total nitrogen flux budget over eight rural sites across eastern Canada, and estimated that HNO_3 constituted less than half of the NO_y flux (46%), and the flux from other measured gaseous nitrogen species ($NO_2 + PAN + PPN$) were also a significant portion (35%). Those new field data suggested that other forms of gaseous nitrogen like NO_2 and PANs instead of HNO_3 can constitute the dominant portion of the NO_y deposition at some sites. As $V_d(NO_2)$ and $V_d(PAN)$ are not evaluated directly due to lack of observations, we compared the simulations between models. Table 2 shows the model estimates of R_c and V_d for NO_2 and PAN during different daytime periods of summer. PAN presented a larger R_c (~200 s m^{-1}) than NO_2 (~120 s m^{-1}). Compared with WDDM, Noah-GEM produced smaller R_c for NO_2 and PAN during the morning and afternoon period, while slighter lager ones during the noon. The differences of R_c between WDDM and Noah-GEM reached a factor of 1.1–1.5 on average, which in turn leads a factor of 1.1–1.3 for V_d.

The NO_y species have various physical and chemical natures, leading to very different behaviors in the deposition process. The $V_d(HNO_3)$ estimated by Noah-GEM is one order of magnitude larger than $V_d(NO_2)$ and $V_d(PAN)$ (Fig. 11), whereas $V_d(NO)$ is close to zero. Dry deposition of NO is usually assumed to be negligible as NO is almost inert to the mesophyll, the surface of canopy, or ground. Significant rates of NO_2 uptake by vegetation through stomata have been observed in chamber experiments (Hanson and Lindberg, 1991). The assumption that V_d of NO_2 is similar to that of O_3 is usually used in deposition models. However, the deposition processes of NO and NO_2 are difficult to quantify in field measurements as NO_x ($NO_x = NO + NO_2$) rapidly interconverts between the surface and the height of flux measurement, which violates the assumption for a constant flux layer. Ideally, the NO_x flux above the canopy should be examined as a whole that is conserved chemically on timescales relevant to turbulent exchange (Wesely, 1989). Noah-GEM estimates R_c for PAN based on molecular diffusivity, solubility, chemical reactivity and comparison to O_3 or SO_2 deposition, leading to a prediction of daily maximum V_d(PAN) on the order of 0.5 cm s^{-1}, almost half of $V_d(O_3)$. Turnipseed et al. (2006) reported the first direct measurement of eddy-covariance fluxes of PAN to a coniferous forest and showed a mean daily maximum value of V_d(PAN) at ~1.2 cm s^{-1}. The findings of fast deposition of PAN (Turnipseed et al., 2006) imply large uncertainties in parameterizing R_c of organic compounds, and also indicate the importance of organic nitrogen in the reactive nitrogen deposition budget. Peak values of $V_d(HNO_3)$ modeled by Noah-GEM ranged from 3 to 6 cm s^{-1}, on the same order with the gradient-method measurements by Meyers et al. (1989) over a dense deciduous forest (2.2 to 6.0 cm s^{-1}) and Sievering et al. (2001) over a conifer forest (7.6 cm s^{-1}).

We estimated the deposition fluxes of individual NO_y species by multiplying the predicted V_d (using $z_0 = 2$ m) with the observed concentrations (Eq. (1)). On average, NO_x, PAN and HNO_3 accounted for 19%, 4%, and 70% of the measured NO_y fluxes, respectively. In the current models we only considered the unidirectional fluxes (deposition), and this assumption is not valid for gases with emission fluxes from the surface. Emissions of NO from soils at HFEMS are negligible (Horii et al., 2005). But Horii et al. (2004) observed bi-directional fluxes of NO_2 and suggested a compensation point for NO_2 near 1.5 ppbv at HFEMS, the ambient concentration below which NO_2 is emitted from stomata. Given that [NO_2] approached this level occasionally during the daytime within the selected period (Fig. 8), the estimate of the contribution of NO_x to NO_y fluxes should be overestimated at some degree. This uncertainty can be narrowed by incorporating a parameterization of the compensation point within the models in the future work. Because the overestimated nocturnal R_a resulted in underestimation of $V_d(HNO_3)$, the contribution of HNO_3 to NO_y fluxes presented here should be considered more of a lower limit.

5. Summary and conclusions

We evaluated the ability of two models (WDDM and Noah-GEM) to calculate $V_d(O_3)$ and $V_d(NO_y)$ against direct observations at HFEMS, and identified key variables/parameters and uncertainties in the two models. WDDM employs Wesely (1989) parameterization for R_c, which uses a simple R_s scheme based on the R_i parameter prescribed for each season and land-cover category. The uncertainty in prescribed R_i dominates the errors in estimating V_d for O_3 and other gases that are controlled by the stomatal pathway. An infinite R_i value for deciduous forest in autumn in the default WDDM was not appropriate and resulted in too low values of $V_d(O_3)$, while using R_i values originally prescribed for summer (70 s m^{-1}) produced better $V_d(O_3)$. More evaluations of WDDM for R_i at different seasons are needed to mitigate the underestimation of $V_d(O_3)$. Several revisions to the

original GEM formulations were justified by comparing the formulations with other literature and also by evaluating modeled surface sensible/latent heat fluxes against observations. Compared with WDDM, Noah-GEM has a more sophisticated R_s scheme considering the response of physiological processes to environmental variables (such as soil moisture, vapor pressure deficit, and CO_2 concentration at the leaf surface) and shows a better ability to capture the variations in $V_d(O_3)$ than WDDM. The models still need to be improved to better represent the nocturnal O_3 dry deposition process.

On the other hand, results showed that $V_d(NO_y)$ calculation was not sensitive to R_s, as expected, because $V_d(NO_y)$ was mainly affected by the rapidly depositing species such as HNO_3 and controlled by the atmospheric resistances (i.e. R_a and R_b). The difference in calculated $V_d(NO_y)$ by WDDM and Noah-GEM was small as these two models produced similar R_a and R_b. WDDM and Noah-GEM agreed well with the observed daytime $V_d(NO_y)$, but underestimated it under nighttime stable conditions. A modest adjustment in the z_0 values can significantly alter and/or improve the predicted $V_d(NO_y)$. Daytime $V_d(NO_y)$ was more sensitive to z_0. These sensitivity tests regarding z_0 and inferior performance of WDDM and Noah-GEM models under stable conditions illustrate the importance and difficulties in modeling the biosphere–atmosphere exchange within the forest canopies, the layer known as roughness sub-layer where the traditional MOST theory is not valid. Therefore, our future model development effort will involve utilizing vertically-varying profiles of mean scalar concentration including chemical species such as PAN, NO and NO_2 or a multi-layer canopy model that explicitly resolves the radiative, dynamical, and thermal transfer within vegetation canopies. Finally, with a combination of the observed concentrations and modeled V_d, it was estimated that NO_x, PAN, and HNO_3 were 19%, 4%, and 70% of the measured NO_y dry deposition fluxes, respectively. Comparison of the simulated R_c and V_d for NO_2 and PAN shows that differences of R_c estimates between WDDM and Noah-GEM were large and would cause differences in V_d reach a factor of 1.1–1.3.

Very few studies were done in the past to extensively focus on evaluating nitrogen-deposition models, which are critical to estimating the surface and atmospheric nitrogen budget in atmospheric chemistry models, primarily due to lack of observations. This is particularly true regarding the WRF-Chem model, because its dry deposition calculation has not been systematically evaluated despite its popularity in atmospheric air quality community. This work is a first step and yet a preliminary study to evaluate the effects of two modules with different treatment of canopy resistance on deposition estimation. The implementation of Noah-GEM calculated V_d in WRF-Chem is underway. And more comprehensive studies at different seasons and locations (for different forest types) will be done in the future.

Acknowledgements

This work was supported by the Natural Science Foundation of China (grant Nos. 40875076, U0833001), the National Program on Key Basic Research Project of China (973) (grant No. 2010CB428504) and the Fundamental Research Funds for the Central Universities. We also gratefully acknowledge the NCAR Advanced Study Program (ASP), BEACHON and Water System Programs. This research also benefited through the NOAA/JCSDA grant (NA06NES4400013), NASA-Terrestrial Hydrology Program and DOE ARM program. The Harvard Forest site is supported by U. S. NSF and DOE BER Program.

Appendix A. Resistance description and formulation comparisons between WDDM and Noah-GEM

Table A.1 gives the definition of each resistance component. Among the three resistances (R_a, R_b and R_c), R_c is generally the most dynamic and difficult to estimate, varying with the properties of the surface and properties of the depositing gas. For many gases such as O_3 and SO_2, R_c is dominant in the deposition process as it is typically the largest in magnitude among the three resistances. However, for very reactive and soluble substances such as HNO_3, R_c can be negligible. Therefore, the deposition of HNO_3 is governed by the atmospheric resistances (R_a and R_b) while the deposition of other species considered in this study is dominated by R_c during daytime.

The deposition may take place through stomata and onto exterior surface (including soil surface). R_c can be generalized from both models discussed here as

$$\frac{1}{R_c} = \frac{1}{R_s + R_m} + \frac{1}{R_{ns}}. \tag{A1}$$

For the R_c-dominant species, a large fraction of the deposition is through direct uptake by vegetation through the stomatal pores (Wesely, 1989).

Table A.2 presents the comparison of the formulations used in WDDM and Noah-GEM. WDDM and Noah-GEM both calculate R_a primarily as a function of surface properties, such as surface roughness, and atmospheric stability through the use of the Monin–Obukhov similarity theory as documented in Chen et al. (1997).

The fundamental difference between WDDM and Noah-GEM exists in the R_s scheme. WDDM employs Wesely (1989) R_c parameterization that estimates R_s based on the parameter of minimum canopy stomatal resistance for water vapor (R_i), which is regulated by two environmental factors, namely solar irradiation (G) and surface air temperature (T_s) (see Eq. (A8)). Niyogi et al. (2009) developed the Gas-exchange Evapotranspiration Model (hereafter referred to as GEM), based on the Ball–Berry stomatal scheme (Eq. (A9)) that describes the response of stomatal conductance for water vapor (g_s, the inverse of R_s) of a single leaf to the rate of net CO_2 uptake (A_n), the relative humidity fraction at the leaf surface (h_s), and CO_2 partial pressure at the leaf surface (C_s). In GEM, a photosynthesis sub-model calculates A_n by considering the effects of *PAR*, canopy temperature and soil moisture in a non-linear way. A leaf boundary layer sub-model calculates C_s and h_s as a function of the ambient CO_2 concentration, relative humidity, air temperature and wind speed. Both sub-models are coupled with the Ball–Berry stomatal sub-model to obtain g_s.

The expressions for R_m and R_{ns} can be found in Wesely (1989) and are not reproduced here for brevity.

Table A.1
Description of the resistance components in the framework of gas dry deposition models.

Symbol	Name	Definition
R_a	Aerodynamic resistance	Turbulent transport between the reference height, z, and the surface.
R_b	Quasi-laminar sub-layer resistance	Mass transfer across the thin layer of air in contact with surface elements.
R_c	Surface resistance	Efficiency of the surface to capture gases.
R_s	Canopy stomatal resistance	A measure of the aperture size of the canopy stomata.
R_m	Mesophyll resistance	Ability of the compounds to be absorbed by the moist cells and mesophyll.
R_{ns}	Non-stomatal resistance	Uptake to other surfaces, including leaf cuticles, bark, soil, or ground litter (grouped together as non-stomatal).

Table A.2
Formulation comparisons between WDDM and Noah-GEM.

WDDM	Noah-GEM
R_a is defined following McRae (1981):	
For stable conditions, $R_a = 0.74(\kappa u_*)^{-1}[\ln(z/z_0) + 4.7(z-z_0)/L]$ (A2a)	$R_a = (\kappa u_*)^{-1}[\ln(z/z_0) - \psi_h]$ (A3)
	Ψ_h is after Paulson (1970):
For neutral conditions, $R_a = 0.74(\kappa u_*)^{-1}\ln(z/z_0)$ (A2b)	For stable conditions, $\psi_h = -5\xi$ (A4a)
and for unstable conditions,	and for unstable conditions,
$R_a = 0.74(\kappa u_*)^{-1}\left\{\ln\left[\frac{(1-9z/L)^{0.5}-1}{(1-9z/L)^{0.5}+1}\right] - \ln\left[\frac{(1-9z_0/L)^{0.5}-1}{(1-9z_0/L)^{0.5}+1}\right]\right\}$ (A2c)	$\psi_h = 2\ln\left[\left(1+x^2\right)/2\right]$ (A4b)
	where
where z_0 is the roughness length for momentum, κ is the von Karman's constant (0.4), u_* is the friction velocity, and L is the Obukhov length.	$\xi = z/L$ (A5)
	$x = (1-16\xi)^{1/4}$ (A6)
R_b is following Wesely and Hicks (1977):	
$R_b = 2(\kappa u_*)^{-1}(S_c/P_r)^{2/3}$, (A7)	
where S_c is the Schmidt number and P_r is the Prandtl number for air (0.72).	
Jarvis-style R_s scheme (Wesely, 1989):	Ball–Berry R_s scheme (Ball et al., 1987):
$R_s = R_i\left\{1+\frac{1}{[200(G+0.1)]^2}\right\}\frac{400}{T_s(40-T_s)}\frac{D_{H_2O}}{D_x}$ (A8)	$g_s = m\frac{A_n h_s}{C_s}P + b$, (A9)
where D_{H_2O} and D_x are the molecular diffusivities for water vapor and for a specific gas x.	where P is the atmospheric pressure, m and b are linear coefficients based on gas exchange considerations.
	$R_s = \frac{1}{g_s \mathrm{LAI}}\frac{D_{H_2O}}{D_x}$ (A10)
R_m, and R_{ns} are after Wesely (1989)	

Appendix B. Formulation updates of GEM

The formulation updates of GEM are presented here, however, all original ones used in GEM, and their descriptions can be found in Appendix A and B of Niyogi et al. (2009).

$$w_e = \mathrm{PAR}\varepsilon(1-\omega_\pi)\left[\left(C_i - \Gamma^*\right)/\left(C_i + 2\Gamma^*\right)\right] \quad \text{(B1)}$$

where w_e is the photosynthesis limiting factor due to amount of PAR absorbed by the leaf chlorophyll, PAR is the photosynthetically active radiation, ε is the quantum efficiency for CO_2 uptake, ω_π is the leaf-scattering coefficient for PAR, C_i is the CO_2 partial pressure (Pa) in the leaf intercellular spaces, Γ^* is the CO_2 compensation point (Pa).

$$S_m = 1 - \frac{2}{3}\left[\frac{w_2 - w_{wilt}}{w_{fc} - w_{wilt}}(0.03^{-\frac{1}{B}} - 1.5^{-\frac{1}{B}}) + 1.5^{-\frac{1}{B}}\right]^{-B} \quad \text{(B2)}$$

where S_m is a soil moisture stress factor, w_2 is the root-level soil moisture content, w_{wilt} and w_{fc} are root-level soil moisture wilting and field capacity values, B is the slope of the soil moisture retention curve.

$$V_m = V_{max} f(T) f(w_2) \quad \text{(B3)}$$

where V_m is the maximum catalystic Rubisco capacity for the leaf , V_{max} is the maximum V_m, $f(T)$ and $f(w_2)$ are the stress functions of temperature and soil moisture, respectively.

$$f(T) = 2^{Q_t}\frac{1}{1+\exp[0.3(T_s - S_2)]}\frac{1}{1+\exp[0.3(S_4 - T_s)]} \quad \text{(B4)}$$

where Q_t is the temperature dependency taken as $0.1(T_s - 298.0)$, T_s is the surface or canopy temperature, S_4 and S_2 are low and high temperature stress parameters.

$$g_m = g_{mp}\left[2^{Q_t}\frac{1}{1+\exp[0.3(T_c - S_2)]}\frac{1}{1+\exp[0.3(S_4 - T_s)]}\right] \times \frac{w_2 - w_{wilt}}{w_{fc} - w_{wilt}} \quad \text{(B5)}$$

where g_m is the mesophyllic conductance, which is based on the modulation of a potentially maximum value (g_{mp}).

$$C_s = C_a - A_n P/g_b \quad \text{(B6)}$$

where C_s is the CO_2 partial pressure at the leaf surface, C_a is the ambient CO_2 partial pressure, A_n is the rate of net CO_2 uptake, P is the atmospheric pressure, and g_b is the leaf boundary conductance.

$$w_2 = \frac{\sum_{i=1}^{3}\mathrm{SMC}(i)\times|\mathrm{SLDPTH}(i)|}{\sum_{i=1}^{3}|\mathrm{SLDPTH}(i)|} \quad \text{(B7)}$$

where SMC is the multiple levels of soil moisture content, SLDPTH is the thicknesses of each soil layer, and the 3rd level of soil reaches to 1 m down from the surface.

Eqs. (B1)–(B7) are used to replace Eqs. (A1b), (B5), (A3), (A4), (A2b), and (B3), and Fig. B1 in Niyogi et al. (2009), respectively.

References

Avissar, R., 1993. Observations of leaf stomatal conductance at the canopy scale: an atmospheric modeling perspective. Boundary-Layer Meteorology 64, 127–148.
Ball, J., Woodrow, I., Berry, J., 1987. A model predicting stomatal conductance and its contribution to the control of photosynthesis under different environmental

conditions. In: Biggins, J. (Ed.), Progress in Photosynthesis Research, vol. IV. Martinus Nijhoff, Dordrecht, pp. 221–224.
Charusombat, U., Niyogi, D., Kumar, A., Wang, X., Chen, F., Guenther, A., Turnipseed, A., Alapaty, K., 2010. Evaluating a new deposition velocity module in the Noah land surface model. Boundary-Layer Meteorology. doi:10.1007/s10546-010-9531-y.
Chen, F., Janjic, Z., Mitchell, K., 1997. Impact of atmospheric surface layer parameterization in the new land-surface scheme of the NCEP mesoscale Eta numerical model. Boundary-Layer Meteorology 185, 391–421.
Chen, F., Dudhia, J., 2001. Coupling an advanced land surface – hydrology model with the Penn State–NCAR MM5 modeling system. part I, model implementation and sensitivity. Monthly Weather Review 129, 569–585.
Chen, F., Zhang, Y., 2009. On the coupling strength between the land surface and the atmosphere: from viewpoint of surface exchange coefficients. Geophysical Research Letters 36. doi:10.1029/2009GL037980.
Cooter, E.J., Schwede, D.B., 2000. Sensitivity of the National Oceanic and Atmospheric Administration multilayer model to instrument error and parameterization uncertainty. Journal of Geophysical Research 105. doi:10.1029/1999JD901080.
Flechard, C.R., Nemitz, E., Smith, R.I., Fowler, D., Vermeulen, A.T., Bleeker, A., Erisman, J.W., Simpson, D., Zhang, L., Tang, Y.S., Sutton, M.A., 2010. Dry deposition of reactive nitrogen to European ecosystems: a comparison of inferential models across the NitroEurope network. Atmospheric Chemistry and Physics Discussions 10, 29291–29348.
Galloway, J.N., Townsend, A.R., Erisman, J.W., Bekunda, M., Cai, Z., Freney, J.R., Martinelli, L.A., Seitzinger, S.P., Sutton, M.A., 2008. Transformation of the nitrogen cycle: recent trends, questions, and potential solutions. Science 320, 889–892.
Grell, G.A., Peckham, S.E., Schmitz, R., McKeen, S.A., Frost, G., Skamarock, W.C., Eder, B., 2005. Fully coupled "online" chemistry within the WRF model. Atmospheric Environment 39, 6957–6975.
Guenther, A., Karl, T., Harley, P., Wiedinmyer, C., Palmer, P.I., Geron, C., 2006. Estimates of global terrestrial isoprene emissions using MEGAN, Model of Emissions of Gases and Aerosols from Nature. Atmospheric Chemistry and Physics 6, 3181–3210.
Hanson, P.J., Lindberg, S.E., 1991. Dry deposition of reactive nitrogen-compounds: a review of leaf, canopy and non-foliar measurements. Atmospheric Environment 25A, 1615–1634.
Harman, I.N., Finnigan, J.J., 2008. Scalar concentration profiles in the canopy and roughness sublayer. Boundary-Layer Meteorology 129, 323–351.
Högström, U., 1996. Review of some basic characteristics of the atmospheric surface layer. Boundary-Layer Meteorology 78, 215–246.
Horii, C.V., Munger, J.W., Wofsy, S.C., Zahniser, M., Nelson, D., McManus, J.B., 2004. Fluxes of nitrogen oxides over a temperate deciduous forest. Journal of Geophysical Research 109. doi:10.1029/2003JD004326.
Horii, C.V., Munger, J.W., Wofsy, S.C., Zahniser, M., Nelson, D., McManus, J.B., 2005. Atmospheric reactive nitrogen concentration and flux budgets at a Northeastern U.S. forest site. Agricultural and Forest Meteorology 133, 210–225.
McRae, G.J., 1981. Mathematical Modeling of Photochemical Air Pollution. Ph.D. Thesis. California Institute of Technology, Pasadena, California.
Meyers, T.P., Finkelstein, P., Clarke, J., Ellestad, T.G., Sims, P.F., 1998. A multilayer model for inferring dry deposition using standard meteorological measurements. Journal of Geophysical Research 103 (D17), 645–661.
Meyers, T.P., Huebert, B.J., Hicks, B.B., 1989. HNO_3 deposition to a deciduous forest. Boundary-Layer Meteorology 49, 395–410.
Michou, M., Laville, P., Serça, D., Fotiadi, A., Bouchou, P., Peuch, V.H., 2005. Measured and modeled dry deposition velocities over the ESCOMPTE area. Atmospheric Research 74, 89–116.
Munger, J.W., Wofsy, S.C., Bakwin, P.S., Fan, S.M., Goulden, M.L., Daube, B.C., Goldstein, A.H., 1996. Atmospheric deposition of reactive nitrogen oxides and ozone in a temperate deciduous forest and a subarctic woodland. 1. Measurements and mechanisms. Journal of Geophysical Research 101, 12639–12657.
Munger, J.W., Fan, S.M., Bakwin, P.S., Goulden, M.L., Goltstein, A.H., Colman, A.S., Wofsy, S.C., 1998. Regional budgets for nitrogen oxides from continental sources: variations of rates for oxidation and deposition with season and distance from source regions. Journal of Geophysical Research 103, 8355–8368.
Niyogi, D.S., Alapaty, K., Raman, S., Chen, F., 2009. Development and evaluation of a coupled photosynthesis-based gas exchange evapotranspiration model, GEM for mesoscale weather forecasting applications. Journal of Applied Meteorology and Climatology 48, 349–368.
Paulson, C.A., 1970. The mathematical representation of wind speed and temperature profiles in the unstable atmospheric surface layer. Journal of Applied Meteorology 9, 857–861.
Sievering, H., Kelly, T., McConville, G., Seibold, C., Turnipseed, A., 2001. Nitric acid dry deposition to conifer forests: Niwot Ridge spruce -fir -pine study. Atmospheric Environment 35, 3851–3859.
Shannon, J.D., Sisterson, D.L., 1992. Estimation of S and NOx–N deposition budgets for the United States and Canada. Water, Air, and Soil Pollution 63, 211–235.
Sparks, J.P., Walker, J., Turnipseed, A., Guenther, A., 2008. Dry nitrogen deposition estimates over a forest experiencing free air CO_2 enrichment. Global Change Biology 14. doi:10.1111/j.1365-2486.2007.01526.x.
Turnipseed, A.A., Huey, L.G., Nemitz, E., Stickel, R., Higgs, J., Tanner, D.J., Slusher, D.L., Sparks, J.P., Flocke, F., Guenther, A., 2006. Eddy covariance fluxes of peroxyacetyl nitrates, PANs and NOy to a coniferous forest. Journal of Geophysical Research 111. doi:10.1029/2005JD006631.
Turnipseed, A.A., Burns, S.P., Moore, D.J.P., Hu, J., Guenther, A.B., Monson, R.K., 2009. Controls over ozone deposition to a high elevation subalpine forest. Agricultural and Forest Meteorology 149, 1447–1459.
Urbanski, S., Barford, C., Wofsy, S., Kucharik, C., Pyle, E., Budney, J., McKain, K., Fitzjarrald, D., Czikowsky, M., Munger, J.W., 2007. Factors controlling CO2 exchange on timescales from hourly to decadal at Harvard Forest. Journal of Geophysical Research – Biogeosciences 112 (G2) G02020.
Wang, X.M., Chen, F., Wu, Z.Y., Zhang, M.G., Tewari, M., Guenther, A., Wiedinmyer, C., 2009. Impacts of weather conditions modified by urban expansion on surface ozone: Comparison between the Pearl River Delta and Yangtze River Delta regions. Advances in Atmospheric Sciences 26, 962–972.
Wesely, M.L., Hicks, B.B., 1977. Some factors that affect the deposition rates of sulfur dioxide and similar gases on vegetation. Journal of the Air Pollution Control Association 27, 1110–1116.
Wesely, M.L., 1989. Parameterization of surface resistances to gaseous dry deposition in regional-scale numerical models. Atmospheric Environment 23, 1293–1304.
Wesely, M.L., Hicks, B.B., 2000. A review of the current status of knowledge in dry deposition. Atmospheric Environment 34, 2261–2282.
Wu, Y., Brashers, B., Finkelstein, P.L., Pleim, J.E., 2003. A multilayer biochemical dry deposition model: 1.Model formulation. Journal of Geophysical Research 108. doi:10.1029/2002JD002293.
Zhang, L., Moran, M., Makar, P., Brook, J., Gong, S., 2002. Modeling gaseous dry deposition in AURAMS: a unified regional air-quality modelling system. Atmospheric Environment 36, 537–560.
Zhang, L., Brook, J.R., Vet, R., 2003. A revised parameterization for gaseous dry deposition in air-quality models. Atmospheric Chemistry and Physics 3, 2067–2082.
Zhang, L., Vet, R., Brook, J.R., Legge, A.H., 2006. Factors affecting stomatal uptake of ozone by different canopies and a comparison between dose and exposure. Science of the Total Environment 370, 117–132.
Zhang, L., Vet, R., O'Brien, J.M., Mihele, C., Liang, Z., Wiebe, A., 2009. Dry deposition of individual nitrogen species at eight Canadian rural sites. Journal of Geophysical Research 114. doi:10.1029/2008JD010640.